PNAS RESEARCH ARTICLE | IMMUNOLOGY AND INFLAMMATION

Regulatory T cells safeguard liver health during metabolic-associated steatohepatitis

Bola S. Hanna[a,1,2], P. Kent Langston[a,1,3], Miguel Marin-Rodero[a], Ricardo N. Ramirez[a,4], Min Wan[b,5], Christophe Benoist[a], and Diane Mathis[a,6]

Affiliations are included on p. 8.

Contributed by Diane Mathis; received December 16, 2025; accepted January 21, 2026; reviewed by Marco Colonna and Jeffrey V. Ravetch

Metabolic-dysfunction-associated steatohepatitis (MASH) is a chronic liver disease driven by the confluence of metabolic stress and destructive inflammation. The immunoregulatory mechanisms that temper this process remain poorly understood. Multipronged data on a complementary pair of murine MASH models and published single-cell RNA-sequencing datasets from MASH patients revealed a critical protective role for Foxp3$^+$CD4$^+$ regulatory T cells (Tregs) in MASH. Tregs progressively accumulated in diseased livers, adopting an activated, nonlymphoid-tissue phenotype marked by expression of the transcription factor Peroxisome Proliferator-Activated Receptor Gamma (PPARγ) as well as a reparative transcriptional program. Punctual ablation of Tregs during established MASH unleashed a catastrophic inflammatory cascade, including exaggerated T-helper (Th)1, Th2, and Th17 responses, expansion of a pathogenic CD8$^+$ T cell population, and hepatocellular injury. Concomitantly, Treg deficiency disrupted key metabolic pathways in the liver, accelerating disease progression. These findings establish Tregs as nonredundant custodians of both immunologic and metabolic homeostasis in the liver, highlighting their promise as targets for temporally tuned immunoregulatory therapies in metabolic liver disease.

regulatory T cells | Tregs | liver | MASH | steatohepatitis

Significance

Metabolic-dysfunction-associated steatohepatitis (MASH) is a chronic liver disease driven by local inflammation and metabolic stress. The regulatory mechanisms that control MASH are poorly understood. Data from a complementary pair of mouse MASH models and published single-cell RNA-sequencing data from MASH patients revealed a critical protective role for Foxp3$^+$CD4$^+$ regulatory T cells (Tregs) in disease progression. Tregs accumulated in diseased livers, adopting an activated phenotype marked by a reparative transcriptional program driven by the transcription factor PPARγ. Ablation of Tregs during established MASH unleashed a catastrophic inflammatory cascade and disrupted key metabolic pathways in the liver, accelerating disease progression. Thus, Tregs are custodians of immunologic and metabolic homeostasis in the liver, highlighting their promise in immunoregulatory therapies of metabolic liver disease.

Treg cells are a specialized subset of CD4$^+$ T lymphocytes that regulates most types of immune response. Beyond their canonical anti-inflammatory role in secondary lymphoid organs, Tregs are found in diverse nonlymphoid tissues, where they not only control local immunologic tenor but also safeguard tissue homeostasis, regulating processes such as metabolism, repair, regeneration, and nociception (1–4). Among these so-called "tissue-Tregs," those located in epididymal visceral adipose tissue (eVAT) are a prototypical example. In aged lean mice, eVAT Tregs are the major component of the local CD4$^+$ T cell compartment, are characterized by a PPARγ-driven transcriptional program, have a clonally expanded T cell receptor (TCR) repertoire shaped by local antigens, and depend on local tissue-derived cues such as interleukin (IL)-33 (1, 5). Through interactions with other immunocytes, stromal cells, and adipocytes, they suppress inflammation, regulate local and systemic metabolism, and control adipogenesis and lipolysis (5–9). Obesity reduces the compartment of eVAT Tregs and compromises their function, thereby promoting adipose-tissue inflammation, insulin resistance, and other features of the "metabolic syndrome" (1, 5, 10).

Metabolic-dysfunction-associated steatohepatitis (MASH) is a related but distinct inflammatory complication of the metabolic syndrome, characterized by steatosis, hepatocellular injury, immunocyte accumulation, and progressive fibrosis (11). While disease initiation is driven by metabolic stress, its chronicity and progression depend on sustained immunologic activation (12). Hepatic CD8$^+$ T cells, particularly a PD1$^+$CXCR6$^+$ "autoaggressive" subset, have been implicated as direct effectors of hepatocyte death (13, 14). The local population of IL-17-producing cells, including Th17 conventional CD4$^+$ T (Tconv) cells, is similarly expanded and promotes steatosis, inflammation, and fibrosis (15–17). In contrast, the role of hepatic Tregs in MASH has been explored only sparingly, and the limited studies available yield conflicting results, some implicating these cells in disease exacerbation, others attributing to them a protective, homeostatic function (18, 19).

The striking parallels between eVAT inflammation in obesity and hepatic inflammation in MASH prompted us to examine the Treg compartment in the liver. To this end, we combined longitudinal and cross-sectional analyses of a complementary pair of dietary mouse models of MASH, including transcriptomic profiling at the population, single-cell, and whole-tissue level. This multipronged approach revealed a dynamic alteration of the hepatic Treg compartment, including the emergence of an activated, PPARγ$^+$ reparative subset.

[1]B.S.H. and P.K.L. contributed equally to this work.

[2]Present address: Department of Immunology Discovery, Genentech, S. San Francisco, CA 94080.

[3]Present address: Department of Pathology, Yale Center for Research on Aging, Yale School of Medicine; New Haven, CT 06510.

[4]Present address: The MED13L Foundation, Park Ridge, IL 60068.

[5]Present address: Pioneering Medicines, Cambridge, MA 02142.

[6]To whom correspondence may be addressed. Email: dm@hms.harvard.edu.

This article contains supporting information online at https://www.pnas.org/lookup/suppl/doi:10.1073/pnas.2536314123/-/DCSupplemental.

Published February 17, 2026.

Functional perturbation experiments demonstrated that Tregs play an indispensable role in constraining hepatic inflammation and preserving metabolic homeostasis during MASH progression.

Results

Tregs Accumulate in the Liver During MASH Development. To probe the role of Tregs in MASH, we turned to two well-established dietary mouse models: the choline-deficient, L-amino acid-defined, high-fat diet (CDAHFD) and the amylin liver NASH (AMLN) diet. The CDAHFD, which combines choline deprivation with a high-fat content and defined amino acid composition, elicits rapid-onset steatosis, inflammation, and fibrosis (20). In contrast, the AMLN diet, enriched in fat, fructose, and cholesterol, induces a slower but steadily progressive form of the disease, characterized by hepatocellular ballooning, chronic inflammation, and fibrotic remodeling (21).

Longitudinal profiling of CDAHFD-fed mice revealed an accumulation of hepatic immunocytes ($CD45^+$ cells) already within the first week after introducing the enriched diet (*SI Appendix*, Fig. S1*A*). Concomitantly, the population of Tregs expanded, both their frequency within the $CD4^+$ T cell compartment and their absolute number (Fig. 1*A*), peaking at week 4 before contracting at later timepoints (Fig. 1*B*). In the slower-evolving AMLN model, the increase in Treg numbers was delayed, becoming particularly evident after 20 wks (Fig. 1*C*), in keeping with the protracted disease course.

To explore whether a similar phenomenon occurs in humans, we interrogated two published single-cell RNA-sequencing (scRNA-seq) datasets from livers of MASH patients (22, 23) (Fig. 1*D* and *SI Appendix*, Fig. S1 *B* and *C*). Focusing our analysis on the $CD4^+$ T cell compartment, we identified *FOXP3*$^+$ cells expressing canonical Treg cell transcripts, including *IL2RA*, *CTLA4*, and *TNFRSF18* (Fig. 1 *D*, *Right* panel). Notably, the Treg

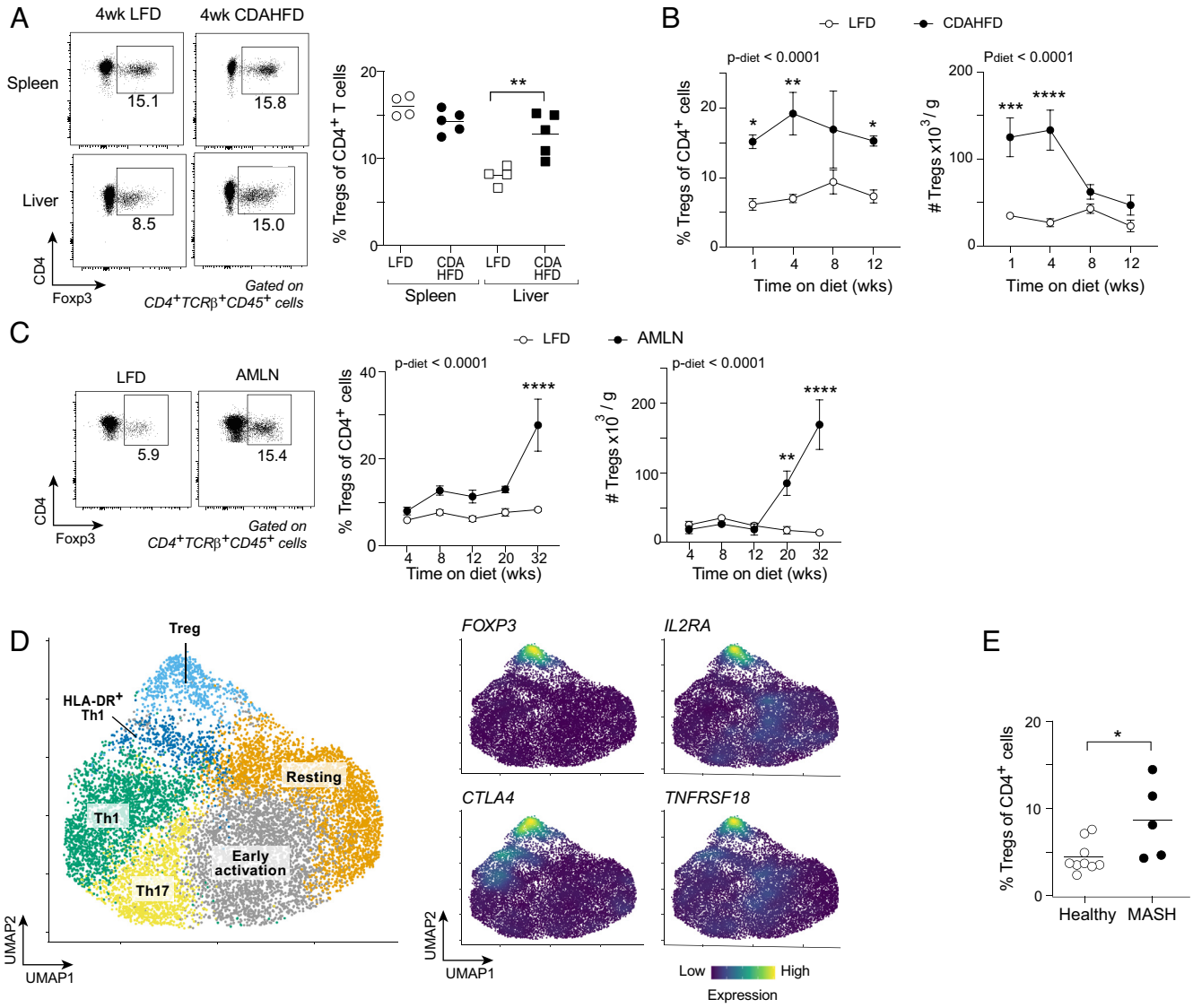

Fig. 1. MASH induces accumulation of Tregs in the liver. (*A*) Representative flow-cytometry plots of Tregs in spleen and liver from mice fed CDAHFD versus LFD for 4 wks. Numbers beside gates indicate the frequencies of gated cells among $CD4^+TCR\beta^+CD45^+$ cells. Summary frequencies are shown to the *Right* (n = 4 to 5). (*B*) Summaries of frequencies of Tregs among all $CD4^+$ T cells and their numbers normalized to liver weights, over 12 wks of CDAHFD versus LFD (n = 4 or 3). (*C*) As per panels A and B, except for livers from mice fed the AMLN diet versus LFD. (*D*) UMAP plot of $CD4^+$ T cells from livers of humans with or without MASH (22, 23). Density plots of expression of canonical Treg transcripts are shown to the *Right*. (*E*) Frequencies of Tregs in livers of patients with MASH versus healthy controls, derived from analysis of published scRNA-seq data (22, 23). $^*P < 0.05$, $^{**}P < 0.01$, $^{***}P < 0.001$, $^{****}P < 0.0001$ by an unpaired Student's *t* test (*A* and *E*) or a two-way ANOVA with Šídák's multiple comparisons test (*B* and *C*). LFD, low-fat diet; CDAHFD, L-amino acid-defined, high-fat diet, AMLN, amylin liver NASH/MASH; MASH Metabolic-dysfunction-associated steatohepatitis.

frequency was significantly elevated in MASH livers relative to that of controls (Fig. 1*E*), echoing the Treg enrichment observed in the CDAHFD and AMLN models.

In Mice With MASH, Liver Tregs Adopt an Activated Phenotype Reminiscent of that of eVAT Tregs. To assess how MASH influences their transcriptional program, we isolated liver Tregs from CDAHFD- or AMLN-fed mice and corresponding controls for population-level RNA-seq analysis. For CDAHFD, we profiled the 8-wk timepoint, which captures the concurrent presence of fibrosis and other key MASH hallmarks such as inflammation and metabolic dysregulation (20). For AMLN, we examined the mice at 20 wks, coinciding with the inflection point of Treg accumulation in our time course (Fig. 1*C*).

In both models, MASH development led to extensive alteration of the liver Treg transcriptional profile: 195 genes upregulated and 154 downregulated in CDAHFD-fed mice; 284 upregulated and 157 downregulated in mice fed the AMLN diet (Fig. 2 *A* and *B*). Transcripts significantly upregulated (padj < 0.05, FC > 2) in both diets encompassed activation markers (*Tnfrsf9, Pdcd1, Cd81 and Cd83*), immunosuppressive mediators (*Il10* and *Fgl2*), early TCR signaling components (*Dusp1, Nr4a2, and Fosl2*), and chemokine receptors associated with tissue residency (*Ccr8 and Cxcr6*). In parallel, genes characteristic of naïve Tregs, including *Ccr7*, *S1pr1,* and *Tcf7*, were significantly downregulated in both models. Pathway-enrichment analysis (Metascape) highlighted immunocyte activation, chemotaxis, and motility pathways in Tregs from CDAHFD-fed and AMLN-diet-fed mice, whereas cell-cycle and replication programs were diminished only in the former case (Fig. 2 *C* and *D*), suggesting a drop in Treg proliferation at this timepoint, which is consistent with the contraction of Treg numbers in later disease stages of this model (Fig. 1*B*).

As expected, liver Tregs from both dietary models acquired the characteristic transcriptional features of nonlymphoid-tissue Tregs (*SI Appendix*, Fig. S2 *A* and *B*). Surprisingly, there was also strong enrichment for the established eVAT-Treg up- and down-signatures, including upregulation of the genes encoding the hallmark transcription factor, PPARγ (Fig. 2 *E* and *F*); in contrast, the lymphoid-tissue Treg signatures were further attenuated (*SI Appendix*, Fig. S2 *A* and *B*). Treg-activation-associated programs were significantly elevated in Tregs from both CDAHFD- and AMLN-diet-fed mice (Fig. 2 *G* and *H*), further confirming that MASH drives the hepatic Treg compartment toward an activated, eVAT-Treg-like state.

The Liver Treg Compartment Is Heterogeneous, With Notable Expansion of a PPARγ$^+$ Subtype in Mice With MASH. Given the extensive transcriptional changes in the hepatic Treg compartment in mice with MASH, we examined their heterogeneity at single-cell resolution, performing scRNA-seq on Tregs sorted from *Foxp3*^{Gfp} reporter mice fed CDAHFD or control diet for 8 wks. Integrated cell-clustering analysis of Tregs from the two conditions resolved four discrete subtypes: "naïve," "*Itgb1*$^+$," "*Pparg*$^-$ reparative" and "*Pparg*$^+$ reparative" (Fig. 3*A*). Gene clustering confirmed the subtype delineations (Fig. 3*B*). The naïve Treg subtype, found in all tissue-Treg compartments so far examined, expressed *Sell*, *Ccr7* and *Tcf7*. The *Itgb1*$^+$ cluster was marked by *S100a10*-, *S100a4*-, *Slamf6*-, and S1P-receptor-encoding (*S1pr1* and *S1pr4*) transcripts. Both reparative clusters expressed diagnostic *Areg* (encoding amphiregulin) and *Il1rl1* (specifying the IL-33 receptor, ST2) transcripts and were enriched for an established reparative-Treg signature (*SI Appendix*, Table S1) (25). While the PPARγ$^-$ reparative subtype expressed higher levels of *Gzmb*, *Ccr2*, *Ccr3,* and *Icos*, its PPARγ$^+$ counterpart was characterized by *Pparg* and *Gata3* expression, as well as high levels of transcripts encoding costimulatory or coinhibitory receptors (*Pdcd1*, *Tnfrsf4*, *Tnfrsf9*, and *Tnfrsf18*) and TCR signaling molecules (*Dusp1*, *Fosl2*, *Junb*, *Nr4a1-3*, *Fos*, and *Jun*), indicative of recent antigenic stimulation (Fig. 3 *B* and *C*). Analysis of the distribution of cells across the UMAP space revealed the naïve and *Itgb1*$^+$ Treg subtypes to predominate in the liver of healthy mice, while CDAHFD feeding drove a pronounced expansion of the two reparative subtypes, most notably that expressing PPARγ (Fig. 3*D*), pointing to a potentially specialized role for these cells in the inflamed liver.

PPARγ Is Dispensable for the Maintenance of Liver Tregs. The surprising appearance of a PPARγ$^+$ Treg cluster in our scRNA-seq dataset prompted us to explore its functional significance. Using *Pparg-Tdt* reporter mice, we confirmed the enrichment of PPARγ$^+$ Tregs in the liver after CDAHFD feeding (Fig. 4*A*). Given PPARγ's well-established nonredundant role in driving eVAT-Treg accumulation and in regulating adipose-tissue inflammation and metabolism (26), we asked whether its absence would similarly compromise liver Tregs in mice with MASH. We generated *Foxp3*^{Cre}.*Pparg*$^{flox/flox}$ (*Pparg*$^{\Delta Treg}$) mice and littermate *Foxp3*^{Cre}.*Pparg*$^{wt/wt}$ (*Pparg*^{wt}) controls, and fed them a CDAHFD or control diet for 8 wks. *Pparg* gene deletion in Tregs had no significant effect on the frequency or absolute number of liver Tregs in either healthy mice or those with MASH (Fig. 4*B*). As illustrated in Fig. 3*C*, high PD-1 display can serve as a marker of the *Pparg*-expressing reparative Treg subtype in the absence of PPARγ. There were moderately fewer PD-1^{hi} Tregs in mice fed CDAHFD but not those on LFD (Fig. 4*C*). Expression of other activation markers, including CD44 and CXCR6, remained unchanged under the two feeding conditions (Fig. 4 *D* and *E*). The distribution of other T cell subsets, both innate and adaptive, was likewise unaffected (*SI Appendix*, Fig. S3). Thus, although PPARγ marks a transcriptionally distinct subset of liver Tregs, it is largely dispensable for their accumulation in the liver, even in the context of MASH-associated inflammatory stress.

Punctual Treg Depletion Exacerbates Hepatitis in Mice With MASH. Thus far, we have established that the development of MASH results in an enriched and distinct hepatic compartment of Tregs. To assess their functional importance, we acutely ablated Tregs in the aforementioned MASH models using *Foxp3.Dtr* transgenic mice, thereby enabling diphtheria toxin (DT)-mediated, temporally-controlled depletion specifically in Tregs.

For the CDAHFD model, mice were fed the enriched diet for 4 wks, followed by three DT injections over 5 d (Fig. 5*A*). This acute loss of Tregs triggered a marked increase in hepatic immunocyte numbers, most prominently numbers of CD4$^+$ T conventional (Tconv) cells and CD8$^+$ T cells (Fig. 5*B*), accompanied by elevated proliferation according to Ki-67 staining (Fig. 5*C*). These effects were not attributable to DT itself, as DT-treated *Foxp3.Dtr*$^-$ littermates showed no such changes (*SI Appendix*, Fig. S4 *A* and *B*). Postdepletion, CD4$^+$ Tconv cells exhibited elevated expression of Tbet, GATA3, and RORγt, supreme regulators of Th1, Th2, and Th17 cell differentiation (Fig. 5*D*). They also produced the corresponding cytokines IFN-γ, IL-4/5/13, and IL-17A (Fig. 5*E*). CD8$^+$ T cells displayed higher levels of PD-1 and CXCR6 (Fig. 5*F*), a phenotype that has been linked to autoaggressive cytotoxic lymphocytes implicated in hepatocyte injury during MASH development (14, 23). Similar results were obtained when Tregs were depleted at 8 wks of CDAHFD feeding (*SI Appendix*, Fig. S4 *C*–*F*). A parallel approach in mice fed the AMLN diet for 20 wks yielded analogous results: robust expansion of inflammatory myeloid populations (Ly6C^{hi} macrophages, neutrophils), increased

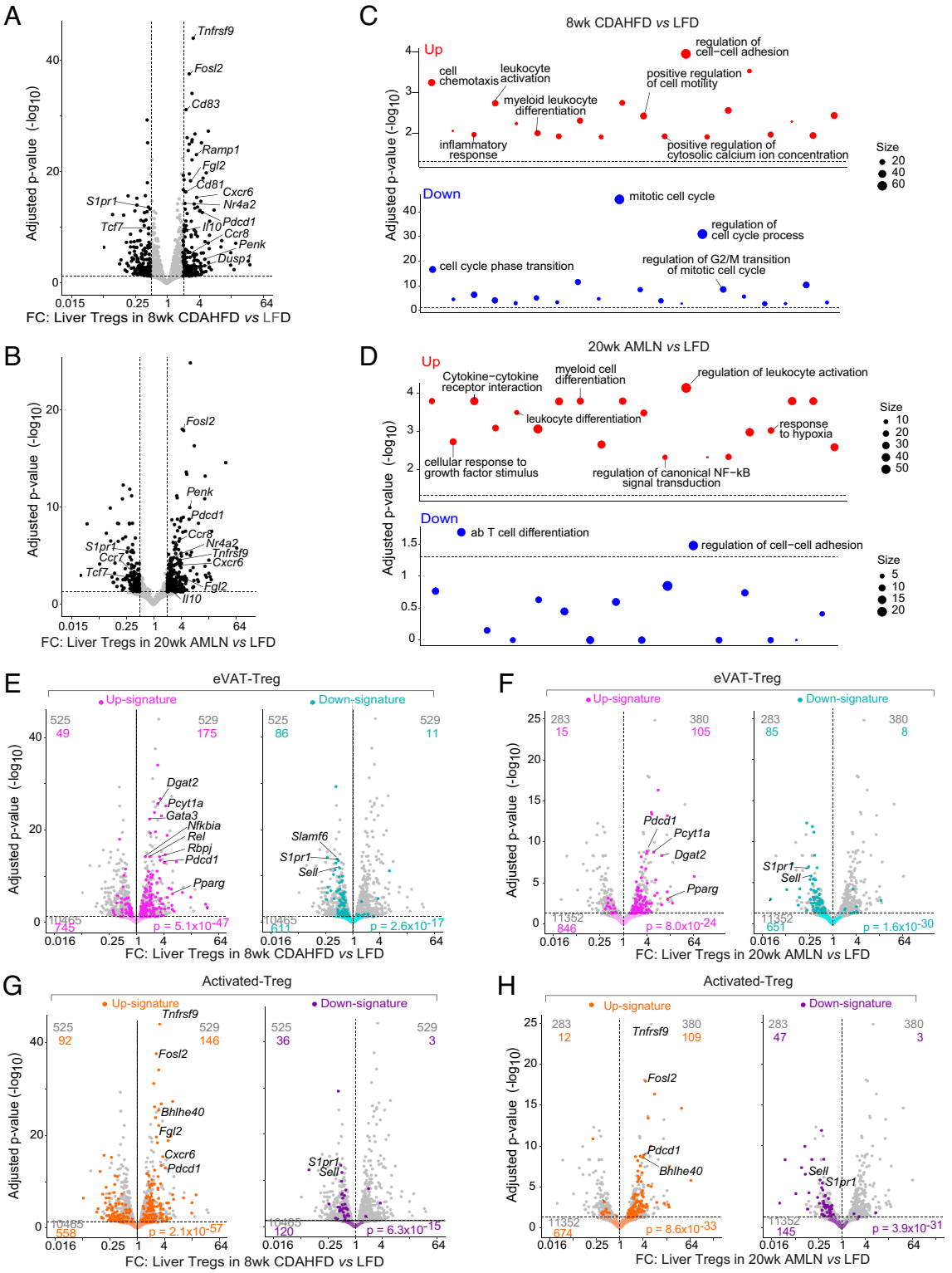

Fig. 2. Liver Tregs adopt an activated, VAT-Treg-like phenotype in mice with MASH. (*A*) Population-level RNA-seq analysis of liver Tregs from mice on CDAHFD versus LFD for 8 wks (n = 3). Differentially expressed genes (padj < 0.05, |FC| ≥ 2) are highlighted; genes of high interest are annotated. (*B*) The same as panel A except for mice on the AMLN diet versus LFD for 20 wks (n = 3). (*C*) Pathway enrichment analysis on the differentially expressed genes highlighted in panel *A*. (*D*) Pathway enrichment analysis on the differentially expressed genes highlighted in panel B. (E) Volcano plots of panel A overlain with genes differentially enriched in Tregs in eVAT versus spleen (1). (*F*) Volcano plots of panel B overlain with genes differentially enriched in Tregs in eVAT versus spleen (1). (*G*) Volcano plots of panel *A* overlain with genes differentially enriched in peripheral activated ($CD44^{hi}CD62L^{lo}$) versus resting ($CD44^{lo}CD62L^{hi}$) Tregs (24). (*H*) Volcano plots of panel *B* overlain with genes differentially enriched in peripheral activated ($CD44^{hi}CD62L^{lo}$) versus resting ($CD44^{lo}CD62L^{hi}$) Tregs (24). *P* values computed by Fisher's exact test (*C*, *D*, *G*, and *H*). eVAT, epididymal visceral adipose tissue. All other abbreviations as per prior figures.

$CD4^+$ Tconv cell and $CD8^+$ T cell numbers (Fig. 5 *G* and *H*), heightened proliferation, and a broad enhancement of Th cell representation (Fig. 5 *I*–*K*). These findings demonstrate, then, that hepatic Tregs play a nonredundant role in restraining liver inflammation during the development of MASH, acting primarily to temper effector T cell responses within the liver.

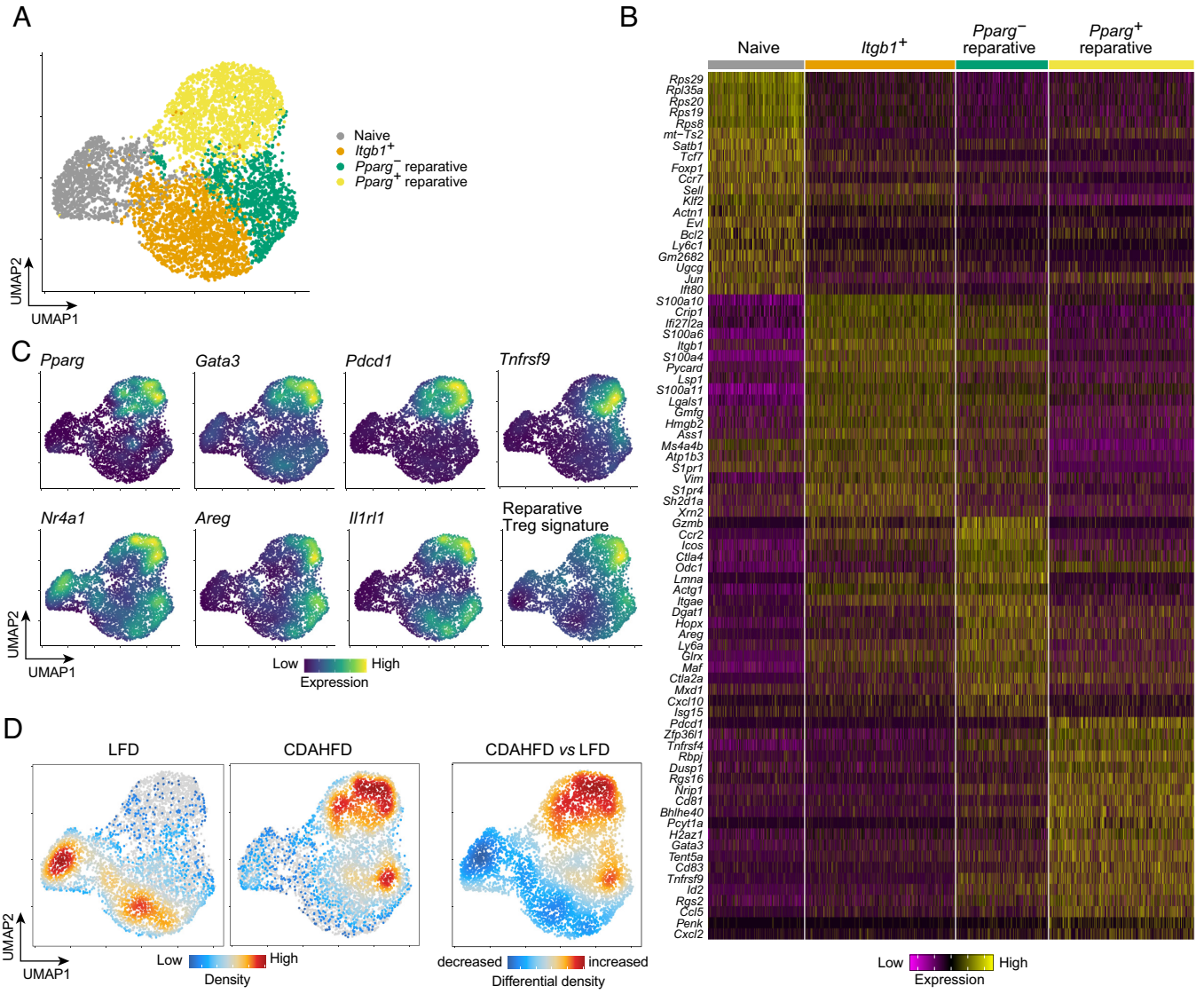

Fig. 3. Liver Tregs are a consortium of subtypes that evolves in MASH. (*A*) UMAP plot of scRNA-seq data from liver Tregs sorted from *Foxp3*^{Gfp} reporter mice fed CDAHFD or LFD for 8 wks. (*B*) Heatmap of the top 20 differentially expressed genes in liver Tregs comparing each cluster with all other clusters. (*C*) Density plots of the expression of genes and gene signatures characteristic of the four liver Treg subtypes delineated in panel *A*. (*D*) Density plots for the two diet groups and differential density between them. All abbreviations as per prior figures.

Treg Depletion Exacerbates Metabolic Dysfunction and Liver Injury in Mice With MASH. To obtain a broad view of how the observed immunological changes impact metabolic programs and liver homeostasis, we performed bulk RNA-seq on livers from CDAHFD-fed mice following Treg depletion. Then, 380 genes were significantly modulated (Padj < 0.05, |FC| > 2) in Treg-deficient livers compared with Treg-positive controls (Fig. 6*A*). Gene-set enrichment analysis showed a strong increase in inflammatory pathways, such as responses to TNFα and IFN (Fig. 6*B*), consistent with our flow cytometric findings (Fig. 5 *E* and *K*). In contrast, metabolic pathways,

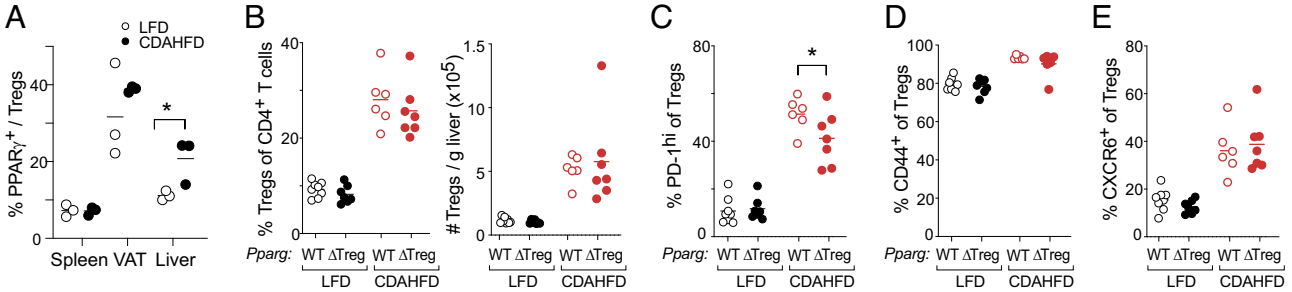

Fig. 4. PPARγ marks liver Tregs that accumulate in MASH, but it is not required for their maintenance. (*A*) Cytofluorometric analysis of PPARγ^{+} Tregs from *Pparg*^{Tdt} reporter mice fed CDAHFD or LFD for 4 wks (n = 3). (*B–E*) Cytofluorometric analysis of liver from *Foxp3*^{Cre}.*Pparg*$^{flox/flox}$ (*Pparg*$^{\Delta Treg}$) mice and littermate *Foxp3*^{Cre}.*Pparg*$^{wt/wt}$ (*Pparg*^{wt}) controls fed CDAHFD or LFD for 8 wks (n = 6). Frequencies and numbers of Tregs (*B*); frequencies of Tregs expressing PD-1 (*C*), CD44 (*D*) or CXCR6 (*E*). *P < 0.05, **P < 0.01, ***P < 0.001, ****P < 0.0001 by an unpaired Student's t test (*A*) or two-way ANOVA with Šídák's multiple comparisons test (*B–E*). All abbreviations as per prior figures.

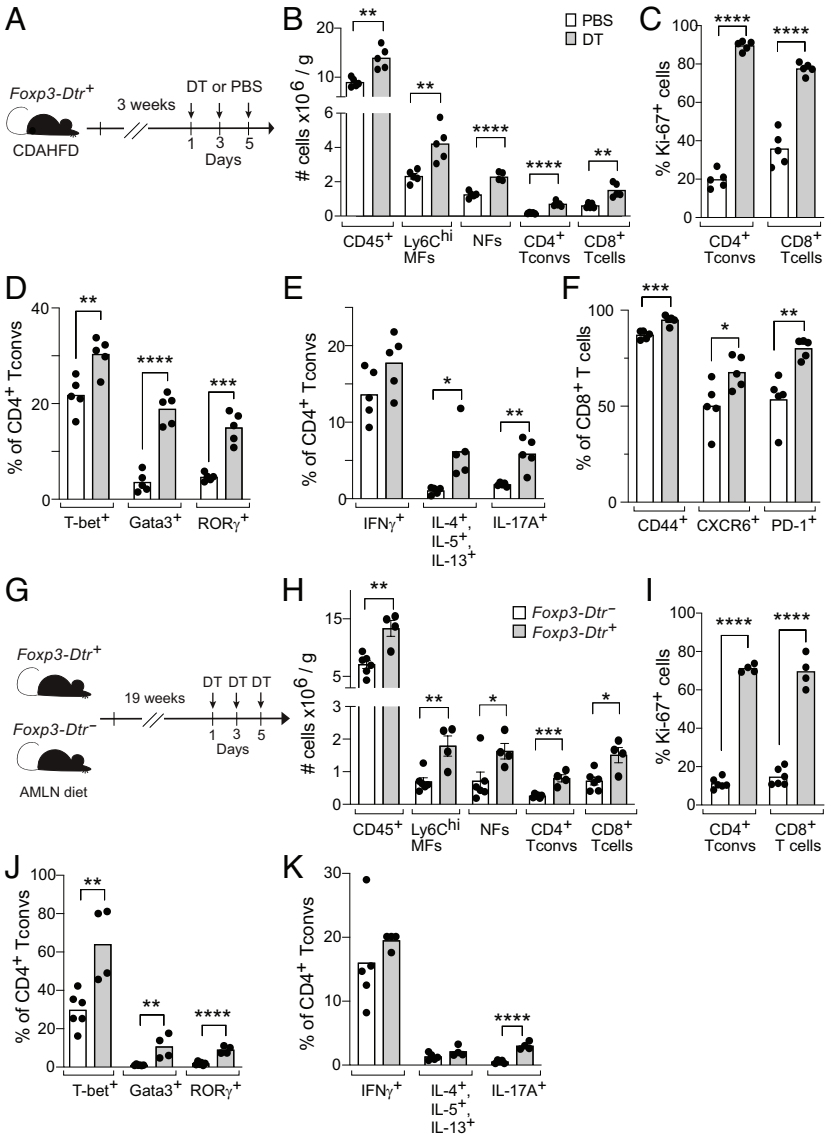

Fig. 5. Tregs restrain hepatitis in mice with MASH. (*A*) Schema for CDAHFD experiments with DT-induced Treg ablation. (*B–F*) Cytofluorometric analysis of livers from *Foxp3.Dtr*$^+$ mice injected with DT or PBS at the end of 4 wks on CDAHFD (n = 5): numbers of the indicated cell types normalized to liver weights (*B*); frequencies of Ki67$^+$ cells among CD4$^+$ Tconv cells and CD8$^+$ T cells (*C*); frequencies of cells expressing Tbet, GATA3, or RORγ among CD4$^+$ Tconv cells (*D*); frequencies of CD4$^+$ Tconv cells producing cytokines corresponding with Th1, Th2, or Th17 cell differentiation (*E*); frequencies of CD44$^+$, CXCR6$^+$, and PD-1$^+$ cells among CD8$^+$ T cells (*F*). (*G–K*) Same as panels *A–E* except for mice fed the AMLN diet for 20 wks *P < 0.05, **P < 0.01, ***P < 0.001, ****P < 0.0001 by an unpaired Student's *t* test. DT, diphtheria toxin; Dtr, diphtheria toxin receptor; MFs, macrophages; NFs, neutrophils; Tconv, T conventional. All other abbreviations as per prior figures.

particularly those related to bile-acid and fatty-acid metabolism, were suppressed. To place these changes in the context of disease progression, we generated a transcriptomic time course from livers of wild-type CDAHFD-fed mice and clustered genes into coregulated modules (*SI Appendix*, Fig. S5 *A* and *B*). One module (C1), enriched for metabolic functions, was highest at baseline and progressively declined over disease unfolding. Three other modules (C2–C4) increased during CDAHFD feeding with distinct kinetics: C2 (protein translation) rose within one week and remained elevated; C3 (ECM deposition/fibrosis) increased steadily to week 12; and C4 (inflammation) peaked at week 8 before declining. Overlaying these signatures on the liver data from mice lacking Tregs revealed that livers from mice lacking Tregs exhibited marked suppression of the C1 metabolic module and strong enrichments of the C2-C4 MASH-associated programs (Fig. 6*C*), suggesting a more advanced disease. These molecular changes were accompanied by elevated measures of plasma Alanine Aminotransferase (ALT) and Aspartate Aminotransferase (AST) in CDAHFD-fed, Treg-deficient mice (Fig. 6*D* and *SI Appendix*, Fig. S5*C*). Similarly, in AMLN-fed mice, Treg depletion increased plasma transaminases and hepatic triglyceride content (Fig. 6*E*). Collectively, these data indicate that Tregs are important for both maintaining hepatic metabolic programs and for limiting inflammation and tissue injury during MASH progression.

Discussion

It is by now well accepted that inflammation is an important element of MASH (12). Key myeloid and lymphoid effector cells have been identified, but we know little about the regulatory cells that keep such inflammation in check in healthy mice and modulate disease progression over the course of MASH development. Our studies have uncovered a substantial accumulation and adaptation of Tregs during the course of MASH in both mice and humans. The numerical increase in hepatic Tregs in mice with MASH, also observed via scRNA-seq in MASH patients, is consistent with recent reports of Treg enrichment in such a setting (27). Beyond this increase, the murine liver Treg compartment adopted an activated, nonlymphoid-tissue-associated phenotype resembling that of eVAT Tregs. The upregulation of TCR signaling genes in Tregs from MASH livers suggests that disease-associated antigens might drive their increased accumulation.

Functionally, hepatic Tregs played a nonredundant role in restraining the activation of both innate and adaptive immunocytes. Acute depletion was sufficient to trigger robust inflammatory responses characterized by increased effector T cell numbers, heightened tissue injury, and metabolic dysregulation. These effects are reminiscent of the loss of control of autoaggressive

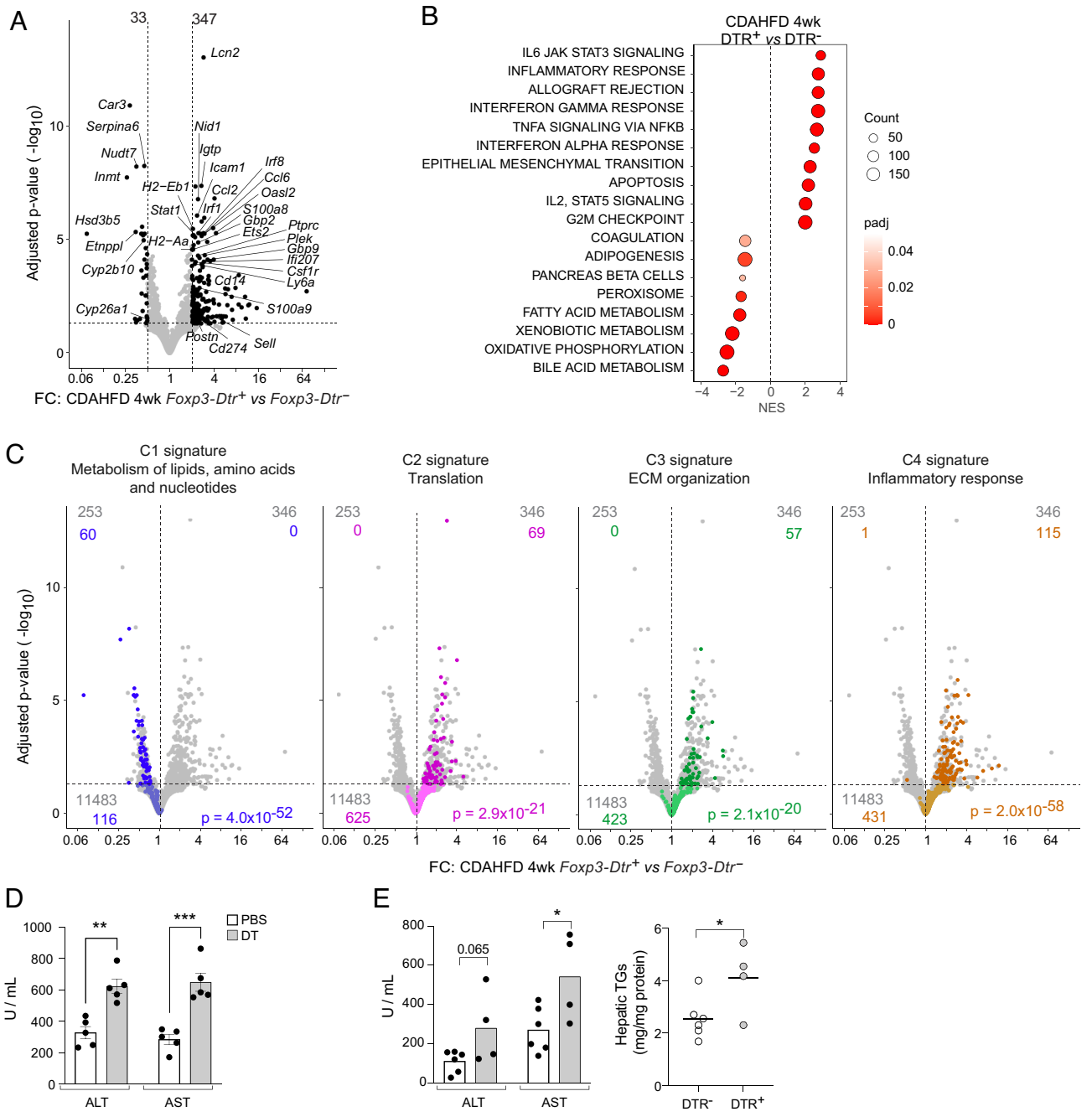

Fig. 6. Tregs guard against metabolic dysfunction and liver damage associated with MASH. (*A*) Bulk RNA-seq analysis of livers from Treg-depleted (*Foxp3.Dtr*$^{+}$; DTR^{+}) vs control (*Foxp3.Dtr*$^{-/-}$, DTR^{-}) mice on CDAHFD for 4 wks (n = 3). Differentially expressed genes (padj < 0.05, |FC| ≥ 2) are highlighted; genes of high interest are annotated. (*B*) Gene Set Enrichment Analysis showing top Hallmark gene sets enriched in livers of DTR^{+} versus DTR^{-} mice after 4 wks on CDAHFD. (*C*) Volcano plots overlain with genes differentially enriched in livers of mice fed CDAHFD compared with LFD-fed controls. Signatures represent coregulated modules identified by clustering significantly modulated genes from a transcriptomic time course (*SI Appendix*, Fig. S5 *A* and *B*). (*D*) Plasma ALT and AST in *Foxp3.Dtr*$^{+}$ mice injected with DT or PBS at the end of 4 wks on CDAHFD (n = 5). (*E*) Plasma ALT and AST and hepatic TG content in DTR^{+} versus DTR^{-} mice fed AMLN diet for 20 wks (n ≥ 4). *P < 0.05, **P < 0.01, ***P < 0.001 by an unpaired Student's t test (*D* and *E*) or p values computed by Fisher's exact test (*C*). ALT, alanine aminotransferase; AST, aspartate aminotransferase; TG, triglyceride. All other abbreviations and statistics as per prior figures.

CD8^{+} T cells previously implicated in antigen-independent hepatocyte killing (14), as well as the unleashing of IL-17-producing cells (15–17). Although the results from our temporally restricted Treg depletion experiments indicate that the detrimental consequences of Treg loss in MASH are most likely driven by the local hepatic Treg compartment, we cannot exclude contributions from systemic effects of Treg depletion, including altered extrahepatic inflammation or perturbations in systemic metabolism. Perturbation of specific tissue-Treg subsets can further address this question. For instance, we previously identified a population of RORγt^{+} Tregs that peaks early in the CDAHFD model and constrains IL-17-mediated inflammation (25). Depletion of this subset accelerated fibrosis, underscoring the importance of Treg-controlled immunologic homeostasis. Our results align with studies showing that ablation of Nr4a1 and Nr4a2 in T cells enhanced liver Treg accumulation and attenuated MASH pathology (19), but contrast with claims of a detrimental role for Tregs in MASH (18, 28). This discrepancy could potentially reflect experimental design, as the constitutive ablation of broad Treg populations in the latter studies likely induced

systemic metabolic alterations that complicate interpretation of liver-specific effects.

Although our data highlight a protective role for Tregs in restraining inflammation, the long-term impact of their sustained accumulation warrants further consideration. Recent work has implicated Treg-derived amphiregulin in the activation of hepatic stellate cells and in fibrogenesis (29). These observations can be reconciled by a model in which the Treg compartment as a whole limits inflammation, particularly in the early stages of MASH, but specific Treg programs or effector subtypes promote fibrosis when present chronically or in excess. However, it is also important to note that, while murine tissue-Tregs are a major source of amphiregulin, its expression in human Tregs is less pronounced (30), raising questions about the importance of this pathway in human MASH.

Although hepatic Tregs in mice with MASH showed increased PPARγ expression, genetic perturbation studies indicated that it was largely dispensable for their accumulation, indicating that PPARγ is a phenotypic rather than functional marker of this population. Notably, PPARγ$^+$ Tregs were the most transcriptionally activated liver Treg subtype, characterized by high expression of genes encoding immunosuppressive and tissue-reparative molecules. Given this profile, it is likely that these cells are involved in the Treg-driven protection in MASH, even if PPARγ itself is not required for their numerical maintenance. Because PPARγ marks tissue-Treg precursors in the spleen (31, 32), the enrichment of PPARγ$^+$ hepatic Tregs could reflect recent recruitment of precursors from secondary lymphoid tissues, although it could also be that local cues in the diseased liver induce its expression. It remains possible that PPARγ exerted functions not assayed in this study, i.e., activities beyond favoring the accumulation of a particular subtype of Tregs. For example, being a transcription factor, PPARγ might upregulate expression of additional repair programs.

Our findings broaden the scope of Treg function in metabolic tissues. Alongside their established roles in eVAT, exercised skeletal muscle, and systemic metabolic homeostasis (5, 26, 32–34), Tregs in the liver emerge as central regulators of the immunologic tone in MASH. These insights have potential therapeutic implications. Strategies to expand or potentiate the Treg compartment, such as administration of low-dose IL-2, engineered forms of IL-2, IL-33, or TNFR2 agonists (35), hold promise, but require precise targeting to avoid unintended proinflammatory Treg counterinfluences or effects on non-Treg populations. In parallel, antigen- or tissue-specific engineered Tregs, generated by endowing an appropriate TCR or chimeric antigen receptor (CAR), offer the possibility of directing Tregs to diseased tissues with high specificity (36). Our results therefore reinforce the therapeutic potential of Tregs in obesity-associated metabolic diseases, while also emphasizing the need for temporal and contextual precision in such manipulations.

Materials and Methods

Mice. C57BL/6 J mice were purchased from Jackson Laboratory. *Foxp3$^{IRES\text{-}GFP}$* (*Foxp3^{Gfp}*) mice (37) were obtained from Dr V. Kuchroo (Brigham and Women's Hospital, Boston, MA). To generate Treg- specific *Pparg*-deficient mice, we crossed *Foxp3^{Cre}* mice (38) (from Dr A. Rudensky, Memorial Sloan Kettering Cancer Center) and B6.*Pparg^{flox}* mice (39). The *Pparg^{Tdt}* reporter line has been previously described (32). *Foxp3-Ires-Gfp.hDtr* (*Foxp3-Dtr)* mice were obtained from Dr A. Rudensky. All animals were maintained under specific pathogen-free conditions in the Harvard Medical School animal facility, and all procedures were approved by the Institutional Animal Care and Use Committee (IS00001257).

Mouse Treatments. To induce MASH, mice were fed either a choline-deficient, L-amino acid-defined, high-fat diet (CDAHFD; A06071309, Research Diets) or an AMLN diet enriched in fat, fructose, and cholesterol (D17010103, Research Diets) starting at 6 to 10 wks of age. Control cohorts received low-fat diets containing either 10 kcal% fat (A08051501, Research Diets) or 13% kcal fat (Picolab Rodent Diet 20, no. 5053).

For Treg depletion, *Foxp3-Dtr*$^+$ mice were injected intraperitoneally with 20 ng DT (Sigma-Aldrich, D0564) per gram body weight in phosphate-buffered saline (PBS). The timing and duration of DT administration for each experiment are presented in the corresponding figure schematics.

Cell Isolation and Flow Cytometry. Livers were excised, minced in Dulbecco's Modified Eagle Medium (DMEM) (Thermo Fisher Scientific) supplemented with collagenase IV (0.5 mg/mL; Gibco), DNase I (150 μg/mL; Sigma-Aldrich), and 1% Fetal Calf Serum (FCS), and incubated at 37 °C for 30 to 45 min with gentle agitation. Single-cell suspensions were stained and analyzed on a FACSymphony flow cytometer (BD Biosciences). Further methodological details are provided in *SI Appendix*, *Materials and Methods*.

RNA Sequencing. For scRNA-seq, hepatic leukocytes were isolated from *Foxp3^{Gfp}* mice fed CDAHFD or control diet for 8 wks. Cells from 4-5 mice per group were pooled, and Tregs were sorted and encapsulated using the Chromium Single Cell 3′ v2 platform (10x Genomics). Sequencing data were processed using the Cell Ranger pipeline (10× Genomics) and analyzed with the Seurat package following established workflows (31, 40). For population-level RNA-seq, Tregs were double-sorted on a MoFlo Astrios or BD Aria II directly into TCL buffer (Qiagen) containing 1% 2-mercaptoethanol (2-ME). For whole-tissue RNA-seq, RNA was isolated from liver using TRIzol (Invitrogen) and the RNeasy Lipid Tissue Mini Kit (Qiagen) according to the manufacturer's instructions, and 2 ng RNA were resuspended in 5 μL of TCL buffer containing 1% 2-ME. Library construction, sequencing, and data processing followed the ImmGen pipeline (www.immgen.org). Additional information on quality control and data analysis is provided in *SI Appendix*, *Materials and Methods*.

Data, Materials, and Software Availability. scRNA-seq and bulk RNA-seq data have been deposited in Gene Expression Omnibus under accession no. GSE314148 (https://www.ncbi.nlm.nih.gov/geo/query/acc.cgi?acc=GSE314148) (41).

ACKNOWLEDGMENTS. We thank K. Hattori, A. Ortiz-Lopez, T. Jayewickreme, and K.R. Smith for experimental assistance; B. Vijaykumar for bioinformatics help; C. Laplace for assistance with graphics; the Harvard Medical School (HMS) Rodent Histopathology Core; and the HMS Immunology Department Flow-Cytometry Core. This work was funded by grants from the NIH (R01 DK092541), the Freedom Together Foundation and Pfizer, Inc. to D.M.

Author affiliations: [a]Department of Immunology, Harvard Medical School, Boston, MA 02115; and [b]Internal Medicine Research Unit, Worldwide Research, Development and Medical, Pfizer Inc., Cambridge, MA 02139

Author contributions: B.S.H., P.K.L., M.W., C.B., and D.M. designed research; B.S.H., P.K.L., and M.M.-R. performed research; R.N.R. analyzed data; M.W., C.B., and D.M. supervised research; and B.S.H., P.K.L., and D.M. wrote the paper.

Reviewers: M.C., Washington University in St Louis School of Medicine; and J.V.R., The Rockefeller University.

Competing interest statement: Reviewer Marco Colonna and corresponding author Diane Mathis are members of the Immunological Genome Project Consortium (ImmGen) that consists of over 25 labs. In that context, they have appeared on the same author list for publications emanating from ImmGen work, but they did not directly collaborate as authors on those manuscripts.

1. A. R. Muñoz-Rojas, D. Mathis, Tissue regulatory T cells: Regulatory chameleons. *Nat. Rev. Immunol.* **21**, 597–611 (2021).
2. D. Burzyn *et al.*, A special population of regulatory T cells potentiates muscle repair. *Cell* **155**, 1282–1295 (2013).
3. E. Midavaine *et al.*, Meningeal regulatory T cells inhibit nociception in female mice. *Science* **388**, 96–104 (2025).
4. A. Mendoza *et al.*, Enkephalin-producing regulatory T cells in the skin restrain local inflammation through control of nociception. *Sci. Immunol.* **10**, eadz6869 (2025).
5. M. Feuerer *et al.*, Lean, but not obese, fat is enriched for a unique population of regulatory T cells that affect metabolic parameters. *Nat. Med.* **15**, 930–939 (2009).
6. R. G. Spallanzani *et al.*, Distinct immunocyte-promoting and adipocyte-generating stromal components coordinate adipose tissue immune and metabolic tenors. *Sci. Immunol.* **4**, eaaw3658 (2019).

7. T. Xiao *et al.*, T_{regs} in visceral adipose tissue up-regulate circadian-clock expression to promote fitness and enforce a diurnal rhythm of lipolysis. *Sci. Immunol.* **7**, eabl7641 (2022).
8. G. Wang *et al.*, Adipose-tissue Treg cells restrain differentiation of stromal adipocyte precursors to promote insulin sensitivity and metabolic homeostasis. *Immunity* **57**, 1345–1359 (2024).
9. M. Marin-Rodero, T. Jayewickreme, C. Benoist, D. Mathis, Seeding of visceral adipose tissue with perinatally generated regulatory T cells shapes the metabolic tenor in mice. *Proc. Natl. Acad. Sci. U.S.A.* **122**, e2518203122 (2025).
10. C. Li *et al.*, Interferon-α-producing plasmacytoid dendritic cells drive the loss of adipose tissue regulatory T cells during obesity. *Cell Metab.* **33**, 1610–1623.e5 (2021).
11. D. Q. Huang *et al.*, Metabolic dysfunction-associated steatotic liver disease in adults. *Nat. Rev. Dis. Primers.* **11**, 14 (2025).
12. T. Huby, E. L. Gautier, Immune cell-mediated features of non-alcoholic steatohepatitis. *Nat. Rev. Immunol.* **22**, 429–443 (2022).
13. M. J. Wolf *et al.*, Metabolic activation of intrahepatic $CD8^+$ T cells and NKT cells causes nonalcoholic steatohepatitis and liver cancer via cross-talk with hepatocytes. *Cancer Cell* **26**, 549–564 (2014).
14. M. Dudek *et al.*, Auto-aggressive $CXCR6^+$ CD8 T cells cause liver immune pathology in NASH. *Nature* **592**, 444–449 (2021).
15. F. Li *et al.*, The microbiota maintain homeostasis of liver-resident γδT-17 cells in a lipid antigen/CD1d-dependent manner. *Nat. Commun.* **7**, 13839 (2017).
16. A. L. Gomes *et al.*, Metabolic inflammation-associated IL-17A causes non-alcoholic steatohepatitis and hepatocellular carcinoma. *Cancer Cell* **30**, 161–175 (2016).
17. T. Fabre *et al.*, Identification of a broadly fibrogenic macrophage subset induced by type 3 inflammation. *Sci. Immunol.* **8**, eadd8945 (2023).
18. H. Wang *et al.*, Regulatory T-cell and neutrophil extracellular trap interaction contributes to carcinogenesis in non-alcoholic steatohepatitis. *J. Hepatol.* **75**, 1271–1283 (2021).
19. D. Aki *et al.*, The Nr4a family regulates intrahepatic Treg proliferation and liver fibrosis in MASLD models. *J. Clin. Invest.* **134**, e175305 (2024).
20. M. Matsumoto *et al.*, An improved mouse model that rapidly develops fibrosis in non-alcoholic steatohepatitis. *Int. J. Exp. Pathol.* **94**, 93–103 (2013).
21. J. R. Clapper *et al.*, Diet-induced mouse model of fatty liver disease and nonalcoholic steatohepatitis reflecting clinical disease progression and methods of assessment. *Am. J. Physiol. Gastrointest. Liver Physiol.* **305**, G483–G495 (2013).
22. P. Ramachandran *et al.*, Resolving the fibrotic niche of human liver cirrhosis at single-cell level. *Nature* **575**, 512–518 (2019).
23. D. Pfister *et al.*, NASH limits anti-tumour surveillance in immunotherapy-treated HCC. *Nature* **592**, 450–456 (2021).
24. Y. Feng *et al.*, A mechanism for expansion of regulatory T-cell repertoire and its role in self-tolerance. *Nature* **528**, 132–136 (2015).
25. B. S. Hanna *et al.*, The gut microbiota promotes distal tissue regeneration via $ROR\gamma^+$ regulatory T cell emissaries. *Immunity* **56**, 829–846 (2023).
26. D. Cipolletta *et al.*, PPAR-γ is a major driver of the accumulation and phenotype of adipose tissue Treg cells. *Nature* **486**, 549–553 (2012).
27. O. P. Martin *et al.*, Single-cell atlas of human liver and blood immune cells across fatty liver disease stages reveals distinct signatures linked to liver dysfunction and fibrogenesis. *Nat. Immunol.* **26**, 1596–1611 (2025).
28. K. Wang *et al.*, ATF4 drives regulatory T cell functional specification in homeostasis and obesity. *Sci. Immunol.* **10**, eadp7193 (2025).
29. T. M. Savage *et al.*, Amphiregulin from regulatory T cells promotes liver fibrosis and insulin resistance in non-alcoholic steatohepatitis. *Immunity* **57**, 303–318 (2024).
30. A. J. Lam *et al.*, Innate control of tissue-reparative human regulatory T cells. *J. Immunol.* **202**, 2195–2209 (2019).
31. C. Li *et al.*, PPARγ marks splenic precursors of multiple nonlymphoid-tissue Treg compartments. *Proc. Natl. Acad. Sci. U.S.A.* **118**, e2025197118 (2021).
32. C. Li *et al.*, TCR transgenic mice reveal stepwise, multi-site acquisition of the distinctive fat-Treg phenotype. *Cell* **174**, 285–299 (2018).
33. D. Kolodin *et al.*, Antigen- and cytokine-driven accumulation of regulatory T cells in visceral adipose tissue of lean mice. *Cell Metab.* **21**, 543–557 (2015).
34. P. K. Langston *et al.*, Regulatory T cells shield muscle mitochondria from interferon-γ-mediated damage to promote the beneficial effects of exercise. *Sci. Immunol.* **8**, eadi5377 (2023).
35. P. J. Eggenhuizen, B. H. Ng, J. D. Ooi, Treg enhancing therapies to treat autoimmune diseases. *Int. J. Mol. Sci.* **21**, 7015 (2020).
36. C. Raffin, L. T. Vo, J. A. Bluestone, T_{reg} cell-based therapies: Challenges and perspectives. *Nat. Rev. Immunol.* **20**, 158–172 (2020).
37. E. Bettelli *et al.*, Reciprocal developmental pathways for the generation of pathogenic effector TH17 and regulatory T cells. *Nature* **441**, 235–238 (2006).
38. Y. P. Rubtsov *et al.*, Regulatory t cell-derived interleukin-10 limits inflammation at environmental interfaces. *Immunity* **28**, 546–558 (2008).
39. T. E. Akiyama *et al.*, Conditional disruption of the peroxisome proliferator-activated receptor gamma gene in mice results in lowered expression of ABCA1, ABCG1, and apoE in macrophages and reduced cholesterol efflux. *Mol. Cell Biol.* **22**, 2607–2619 (2002).
40. E. Kiner *et al.*, Gut $CD4^+$ T cell phenotypes are a continuum molded by microbes, not by T_H archetypes. *Nat. Immunol.* **22**, 216–228 (2021).
41. B. S. Hanna *et al.*, Data from "Regulatory T cells safeguard liver health during metabolic-associated steatohepatitis". GEO. https://www.ncbi.nlm.nih.gov/geo/query/acc.cgi?acc=GSE314148. Deposited 17 December 2025.

SI FIGURE LEGENDS

Fig. S1. Accumulation of immunocytes and Tregs in MASH livers

(A) Number of $CD45^+$ cells, normalized to liver weights, over 12 weeks of CDAHFD versus LFD (n=3-4).

(B-C) scRNA-seq analysis of $CD4^+$ T cells from livers of humans with or without MASH (7, 8). (B) Density plots for healthy and MASH groups, and the differential density between them. (C) Density plots of the expression of genes characteristic of the different $CD4^+$ T cell subtypes delineated in Fig. 1D.

****$p < 0.0001$ by 2-way ANOVA with Šídák's multiple comparisons test (A).

Fig. S2. Liver Tregs in MASH upregulate the established pan-tissue-Treg signature.

RNA-seq analysis of liver Tregs from mice (n=3) on CDAHFD versus LFD for 8wks (A) or AMLN versus LFD for 20wks (B). Volcano plots overlain with genes differentially enriched in Tregs found in nonlymphoid tissues (shared across VAT, skin, liver, skeletal muscle, brain and intestines) versus spleen (17). *p* values computed by Fisher's exact test.

Fig. S3. Myeloid-cell infiltration and activation of conventional $CD4^+$ T cells and $CD8^+$ T cells are unaffected by Treg-specific loss of PPARγ.

(A-D) Cytofluorometric analysis of livers from *Foxp3*^{Cre}.*Pparg*$^{flox/flox}$ (*Pparg*$^{\Delta Treg}$) mice and littermate *Foxp3*^{Cre}.*Pparg*$^{wt/wt}$ (*Pparg*^{wt}) controls fed CDAHFD or LFD for 8wk (n=6): numbers of total (A) and $Ly6C^{hi}$ (B) MFs, as well as frequencies of $CD44^+$, $CXCR6^+$, and $PD\text{-}1^+$ cells among $CD4^+$ (C), and $CD8^+$ (D) T cells.

Fig. S4. Tregs restrain hepatitis in mice with MASH.

(A-B) Cytofluorometric analysis of livers from *Foxp3.Dtr*$^{+}$ mice and littermate *Foxp3.Dtr*$^{-}$ controls fed CDAHFD diet for 4 weeks (n≥3): numbers of CD45^{+} immunocytes, Ly6C^{hi} MFs, NFs, CD4^{+} Tconv cells, and CD8^{+} T cells normalized to liver weights (A); frequencies of Ki67^{+} cells among CD4^{+} Tconv cells and CD8^{+} T cells (B).

(C-F) Cytofluorometric analysis of livers from *Foxp3.Dtr*$^{+}$ mice injected with DT or PBS at the end of 8wks on CDAHFD (n≥4): numbers of CD45^{+} immunocytes, Ly6C^{hi} MFs, NFs, CD4^{+} Tconv cells, and CD8^{+} T cells normalized to liver weights (C); frequencies of Ki67^{+} cells among CD4^{+} Tconv cells and CD8^{+} T cells (D); frequencies of cells expressing T-bet, GATA3, or RORγ among CD4^{+} Tconv cells (E); frequencies of CD4^{+} Tconv cells producing cytokines corresponding to Th1, Th2 or Th17 cell differentiation (F).

*p < 0.05, **p < 0.01, ***p < 0.001, ****p < 0.0001 by an unpaired Student's t-test.

Fig. S5. Tregs guard against metabolic dysfunction and liver damage associated with MASH.

(A-B) Whole-liver RNA-seq timecourse analysis from mice (n=2-3) on CDAHFD versus LFD for up to 12wk. (A) k-means clustering of differentially expressed genes (Padj <0.05, |FC| >2). To the right of each cluster: numbers of co-regulated genes and top pathways from enrichment analysis (Metascape). (B) Relative median expression of each cluster in CDAHFD- versus LFD-fed groups over time.

(C) Plasma ALT and AST levels in *Foxp3.Dtr*$^{+}$ mice injected with DT or PBS at the end of 8wks on CDAHFD (n≥4).

Supplementary Figure 1

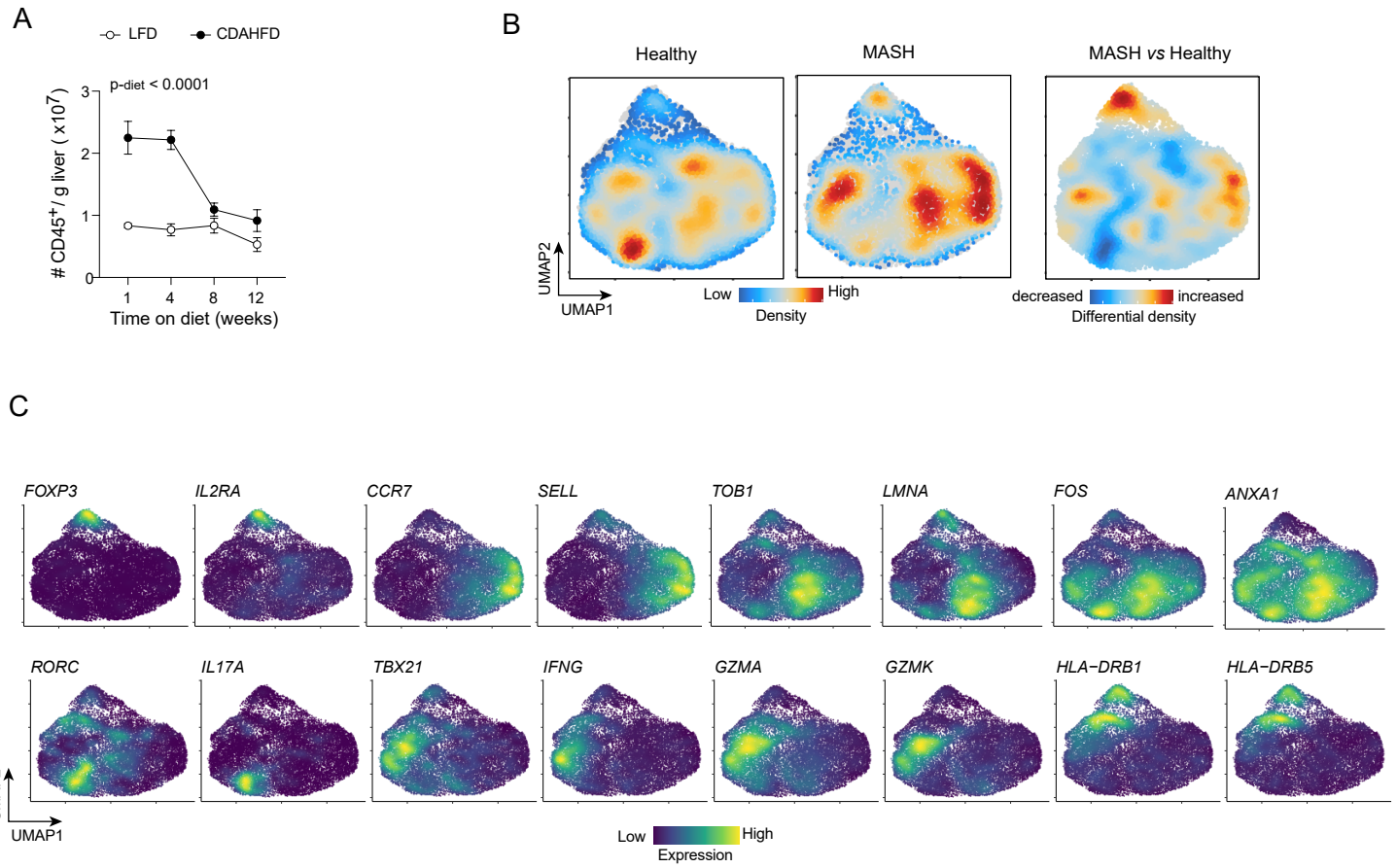

Supplementary Figure 2

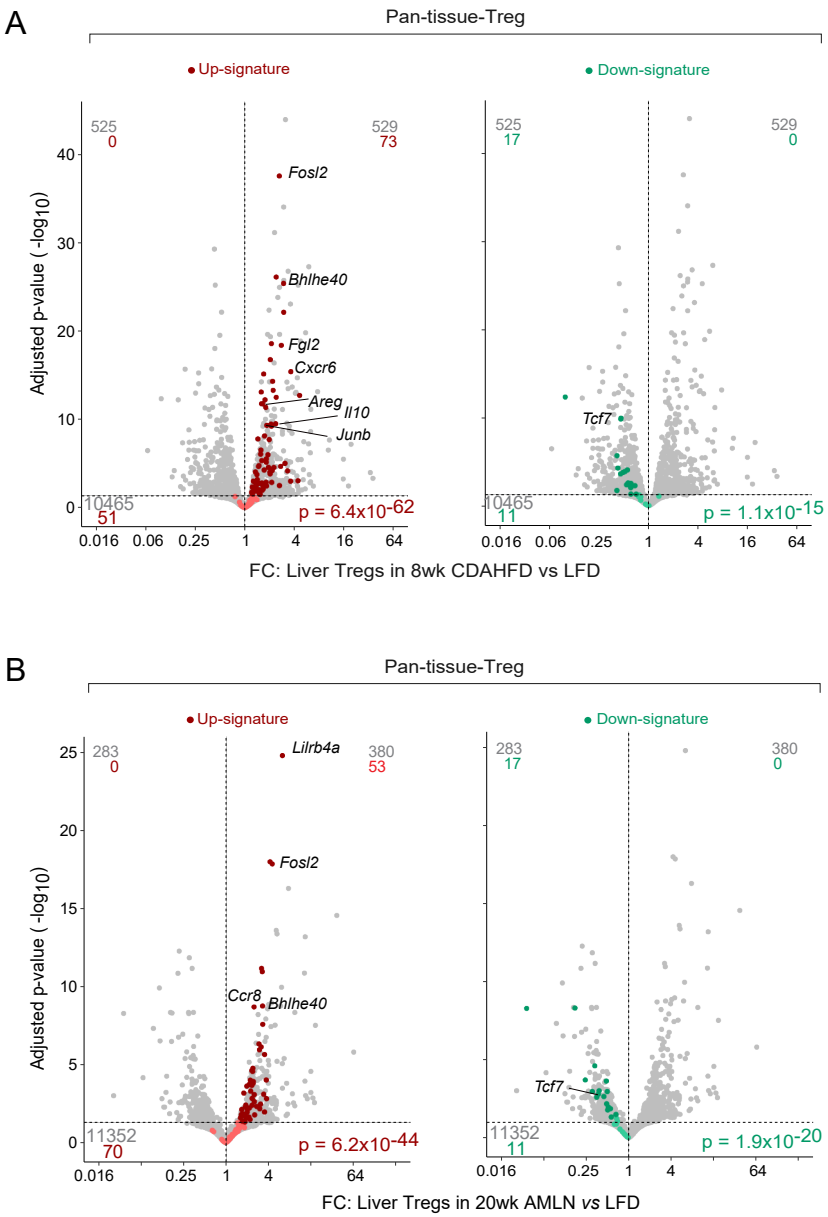

Supplementary Figure 3

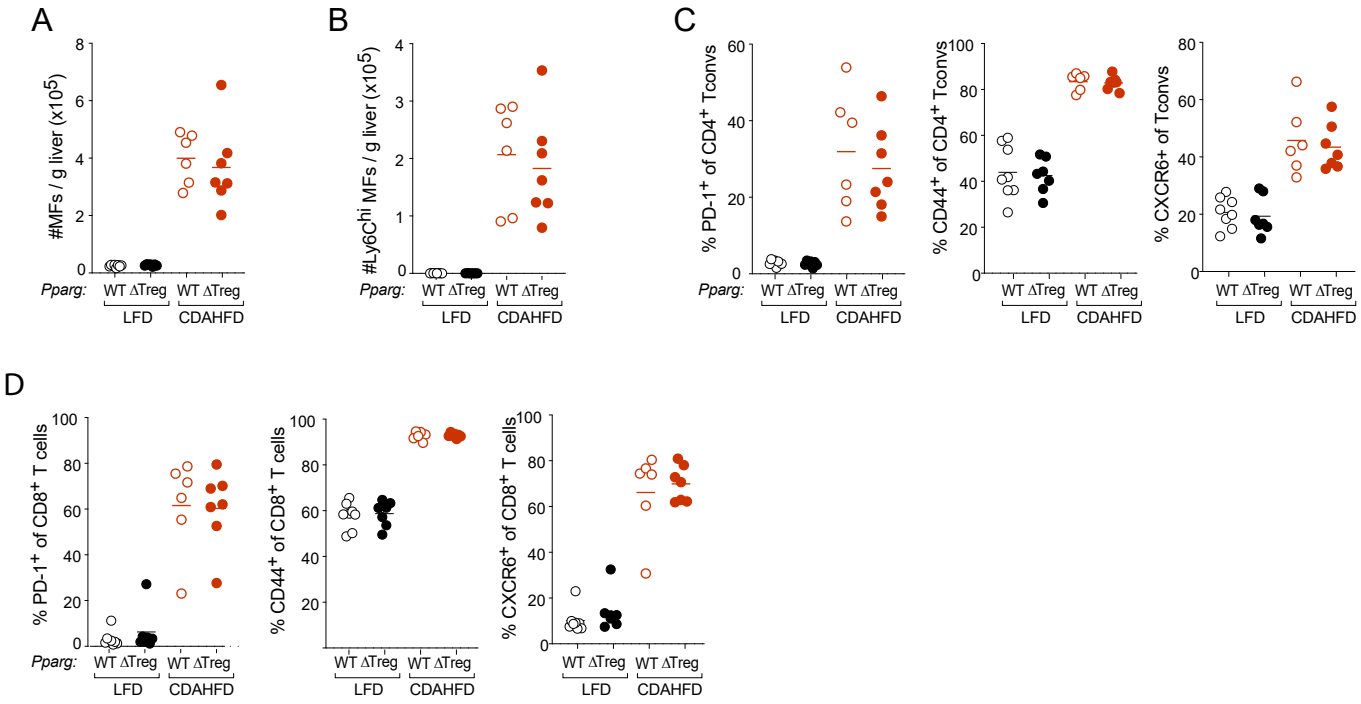

Supplementary Figure 4

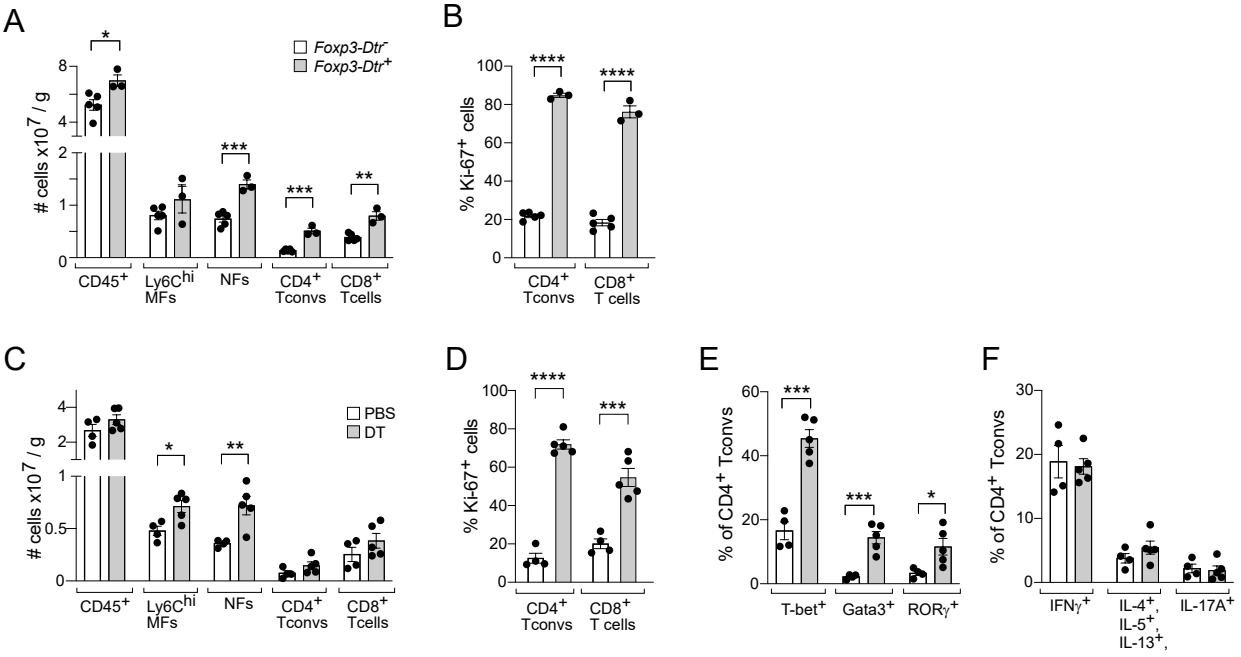

Supplementary Figure 5

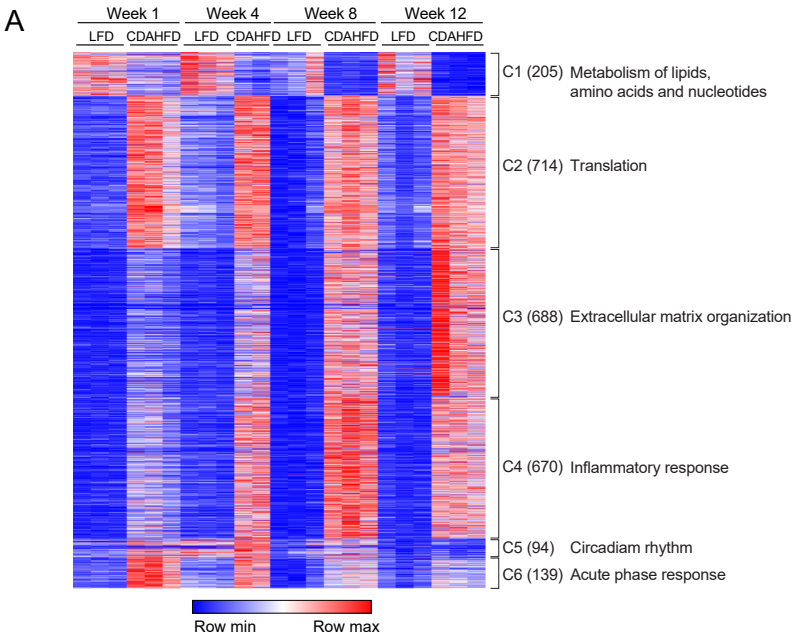

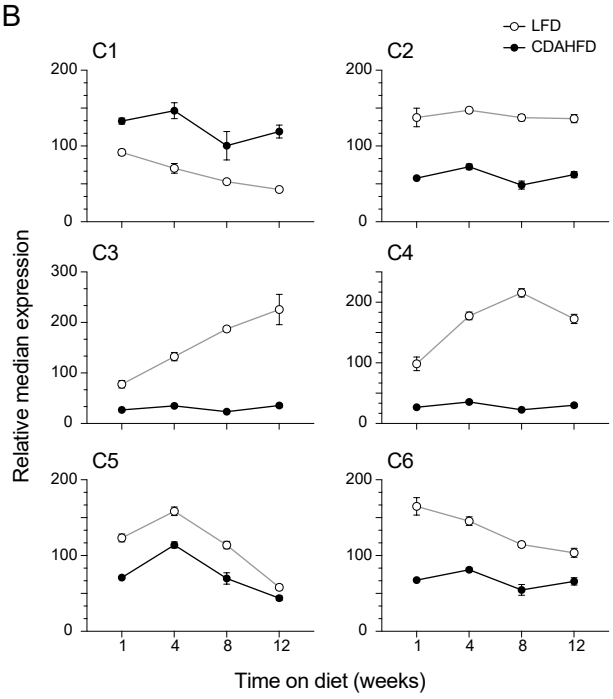

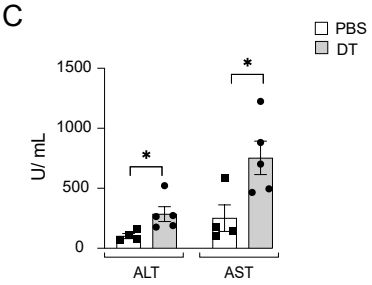

Table S1. Reparative-Treg signature genes from regenerating skeletal muscle (14).

Ikzf2	*Pglyrp1*
Tnfrsf4	*Bcl2a1b*
Cd83	*Fam110a*
Tnfrsf9	*Nfkbid*
Cd74	*Gramd3*
Nfkbia	*Nfkb1*
Areg	*Gadd45b*
Cd81	*Tgif1*
Tnfrsf18	*Tgfb1*
Jund	*Snx18*
Gpx4	*Tspan13*
Rel	*Ctsz*
Ubald2	*Stx11*
Slc16a3	*Odc1*
Id2	*Gata3*
Fam46a	*Hif1a*
Cebpb	*Vgll4*
Traf1	*Syngr2*
Klrg1	*Orai1*
Itm2c	*Cycs*
Nr4a1	*Zfp36l1*
Ifrd1	*Sdf4*
Zc3h12a	*Hilpda*
Slc25a19	*Batf*
Il2ra	*Rhoc*
Icam1	*Gem*
Ccnd2	*Coq10b*
Rrad	*Kdm6b*
Ecm1	*Arl5c*
H2afz	